



# HHS Public Access

## Author manuscript

*Nat Struct Mol Biol.* Author manuscript; available in PMC 2016 March 28.

Author Manuscript

Author Manuscript

Author Manuscript

Author Manuscript

Published in final edited form as:

*Nat Struct Mol Biol.* 2015 July ; 22(7): 547–554. doi:10.1038/nsmb.3038.

## Syntaxin Opening by the MUN Domain Underlies the Function of Munc13 in Synaptic Vesicle Priming

Xiaoyu Yang<sup>1,7</sup>, Shen Wang<sup>1,7</sup>, Yi Sheng<sup>1,7</sup>, Mingshu Zhang<sup>2</sup>, Wenjuan Zou<sup>3</sup>, Lijie Wu<sup>4</sup>, Lijun Kang<sup>3</sup>, Josep Rizo<sup>5</sup>, Rongguang Zhang<sup>2,4</sup>, Tao Xu<sup>1,2,6</sup>, and Cong Ma<sup>1</sup>

<sup>1</sup>Key Laboratory of Molecular Biophysics of the Ministry of Education, College of Life Science and Technology, Huazhong University of Science and Technology, Wuhan, China

<sup>2</sup>National Laboratory of Biomacromolecules, Institute of Biophysics, Chinese Academy of Sciences, Beijing, China

<sup>3</sup>Institute of Neuroscience, Zhejiang University, Hangzhou, China

<sup>4</sup>Institute of Biochemistry and Cell Biology, Shanghai Institutes for Biological Sciences, Chinese Academy of Sciences, Shanghai, China

<sup>5</sup>Department of Biophysics, Biochemistry, and Pharmacology, University of Texas Southwestern Medical Center, Dallas, Texas, USA

<sup>6</sup>College of Life Sciences, University of Chinese Academy of Sciences, Beijing, China

### Abstract

UNC-13-Munc13s play a central function in synaptic vesicle priming through their MUN domains. However, it is unclear whether this function arises from the ability of the MUN domain to mediate the transition from the Munc18-1-closed syntaxin-1 complex to the SNARE complex *in vitro*. The crystal structure of *rat* Munc13-1 MUN domain now reveals an elongated, arch-shaped architecture formed by  $\alpha$ -helical bundles, with a highly conserved hydrophobic pocket in the middle. Mutation of two residues (NF) in this pocket abolishes the stimulation caused by the Munc13-1 MUN domain on SNARE complex assembly and on SNARE-dependent proteoliposome fusion *in vitro*. Moreover, the same mutation in UNC-13 abrogates synaptic vesicle priming in *C. elegans* neuromuscular junctions. These results strongly support the notion that orchestration of syntaxin-1 opening and SNARE complex assembly underlies the central role of UNC-13-Munc13s in synaptic vesicle priming.

---

Correspondence should be addressed to C.M. (cong.ma@mail.hust.edu.cn) or T.X. (xutao@ibp.ac.cn).

<sup>7</sup>These authors contributed equally to this work

**Accession Code.** The coordinates of MUN<sup>933</sup> have been deposited in the Protein Data Bank with accession code 4Y21.

### AUTHOR CONTRIBUTIONS

C.M., M.Z., L.W. and R.Z. performed the structural biology experiments; X. Y. and S. W. generated all mutants used in this study and performed *in-vitro* experiments of SNARE complex assembly and liposome fusion. Y.S., W.Z. and L.K. performed *in-vivo* electrophysiology experiments; T.X. and C.M. conceived the experiments; J.R., T.X. and C.M. wrote the paper.

### COMPETING INTERESTS STATEMENT

The authors declare no competing financial interests.

Neurotransmitter release mediated by  $\text{Ca}^{2+}$ -triggered synaptic vesicle exocytosis is a fundamental process for synaptic transmission. This process is tightly regulated by multiple proteins that form the release machinery. The core machinery includes the neuronal SNAREs syntaxin-1, SNAP-25 and synaptobrevin, as well as the Sec1-Munc18 (SM) protein Munc18-1<sup>1–4</sup>. These proteins are conserved from yeast to human and play key functions in most types of intracellular membrane fusion. The SNAREs play a central role in membrane fusion by forming tight SNARE complexes through their SNARE motifs, which forces the vesicle and plasma membranes into close proximity<sup>5–8</sup>. Munc18-1 orchestrates SNARE complex assembly through its interactions with the SNAREs. For instance, Munc18-1 locks syntaxin-1 in a closed conformation that involves intramolecular binding of its N-terminal H<sub>abc</sub> domain and its SNARE motif, gating entry of syntaxin-1 into the SNARE complex<sup>9–11</sup>. Munc18-1 also interacts with an N-terminal sequence of syntaxin-1 called the N-peptide and with the assembled SNARE complex containing an open conformation of syntaxin-1, which may help catalyzing membrane fusion<sup>12–14</sup>. These multiple interactions, which coordinate syntaxin-1 opening and SNARE complex assembly, are believed to be spatially and timely modulated by other key proteins to enable the exquisite regulation of neurotransmitter release.

Particularly important among these proteins are UNC-13-Munc13s, which are large (ca. 200 kDa) multidomain proteins from presynaptic active zones where vesicles are released<sup>15</sup>. Physiological data showed that UNC-13-Munc13s are crucial components of the release machinery, as release is totally abolished in neurons lacking these proteins, and that UNC-13-Munc13s play a central function in synaptic vesicle priming<sup>16–19</sup>. This function relies on an autonomously folded C-terminal region of UNC-13-Munc13s called the MUN domain (Fig. 1), which is regarded as the minimal module required for the crucial vesicle priming function of UNC-13-Munc13s<sup>20–22</sup>. The finding that syntaxin-1 bearing a so called ‘LE mutation’ that helps opening syntaxin-1 partially rescues release in *unc-13* nulls in *C. elegans* suggested that UNC-13-Munc13s are involved in opening syntaxin-1<sup>23</sup>. However, it was unclear whether direct physical interactions between UNC-13-Munc13s and the SNAREs or Munc18-1 underlie this function. Note for instance that the syntaxin-1 LE mutant also rescued the phenotype observed in the absence of Unc10-RIMs<sup>24</sup>, which are active zone proteins with functions that are coupled to UNC-13-Munc13s<sup>1</sup>. A direct role for the UNC-13-Munc13s in opening syntaxin-1 was strongly supported by recent *in-vitro* studies showing that the Munc13-1 MUN domain accelerates the transition from the Munc18-1-closed syntaxin-1 complex to the SNARE complex<sup>15</sup> and stimulates SNARE-mediated liposome fusion<sup>25</sup>. However, the biological relevance of these findings has not been tested with physiological experiments *in vivo*.

Sequence analyses indicated that the UNC-13-Munc13 MUN domain is homologous to subunits from diverse tethering factors involved in traffic at multiple membrane compartments, such as the exocyst, GARP, COG and Dsl1p complexes<sup>26</sup>. This homology and the crystal structures available for some of these tethering factors<sup>27</sup>, particularly that of Sec6p<sup>28</sup>, suggested that the UNC-13-Munc13 MUN domain contains four subdomains (termed A–D). Indeed, the crystal structure of the region of the Munc13-1 MUN domain spanning the CD subdomains (MUN-CD) revealed a striking structural similarity with the

tethering factors<sup>29</sup>, suggesting that UNC-13-Munc13s might play a role in vesicle tethering through the MUN domain in addition to functioning in synaptic vesicle priming. However, no three-dimensional structure of an entire UNC-13-Munc13 MUN domain has been described and the unavailability of such structure hinders studies involving structure-activity relationships to test the biological relevance of the activity of the MUN domain in opening syntaxin-1 *in vitro* or of its putative function in tethering. It is also worth noting that the structure of the UNC-13-Munc13 MUN domain is the only one lacking for a central component of the neurotransmitter release machinery, as structures have been described for other key components such as the three neuronal SNAREs, Sec1-Munc18s, syntaptotagmin-1 and complexins [reviewed in<sup>30</sup>].

To shed light on the way in which UNC-13-Munc13s regulates syntaxin-1 opening and vesicle priming, we have determined the crystal structure of the Munc13-1 MUN domain at 2.9 Å resolution. Using *in-vitro* FRET and reconstitution experiments, we have identified two highly conserved residues located in the middle of the MUN domain as key sites that mediate opening of syntaxin-1 and SNARE complex assembly. Furthermore, electrophysiological data recorded at cholinergic neuromuscular junctions (NMJs) of *C. elegans* confirm that these two residues are important for both spontaneous and evoked neurotransmitter release, reflecting a critical role in vesicle priming. These results provide compelling evidence that the activity of the MUN domain in stimulating the transition from the Munc18-1-closed syntaxin-1 complex to the SNARE complex *in vitro* underlies the crucial function of UNC-13-Munc13s in synaptic vesicle priming *in vivo*.

## RESULTS

### Crystal structure of Munc13-1 MUN domain

The Munc13-1 MUN domain (residues 859–1531, Fig. 1) is regarded as the minimal module required for the activity of Munc13-1 in synaptic vesicle priming<sup>20</sup>. As mentioned above, structure-based sequence alignments using the available structures of tethering factors homologous to Munc13-1<sup>26</sup> indicate that the MUN domain contains four subdomains termed AD and identified a highly conserved sequence on the C-terminal region of the MUN domain (MUN-CD, residues 1148–1531), aiding in the elucidation of the crystal structure of the MUN-CD region<sup>29</sup>. However, the ability of MUN-CD in opening syntaxin-1 is strongly impaired, consistent with physiological data showing that a fragment (residues 1045–1531) encompassing the MUN-CD region lost its function in rescuing neurotransmitter release<sup>20</sup>. These data imply that the N-terminal portion of the MUN domain (called MUN-AB, residues 859–1147) is indispensable for the priming activity of the MUN domain. Thus, we aimed to crystallize the entire MUN domain containing its A-D subdomains.

Previously, by removing a flexible loop (residues 1408–1452), we successfully improved the yield and solubility of the MUN domain<sup>15</sup> (referred to as MUN\*, residues 859–1407, EF, 1453–1531, Fig. 1), but we were still not be able to obtain high-quality crystals of MUN\* for its structure determination. To solve this problem, we designed a series of truncations of MUN\* (data not shown). Among these truncations, a fragment lacking the first 74 residues on the N-terminus of MUN\* (referred to as MUN<sup>933</sup>, residues 933–1407, EF, 1453–1531,

Fig. 1) was finally crystallized. The MUN<sup>933</sup> structure was determined and refined to 2.9 Å in resolution (**Online Methods**, Fig. 2a and Table 1) and the crystals contained one molecule per asymmetric unit.

The structure of MUN<sup>933</sup> exhibits an elongated shape spanning 150 Å in length. Consecutive helices pack against each other in mixed antiparallel or parallel manner and stabilize the whole structure by inter-helical interactions. MUN<sup>933</sup> is composed of helical-bundle subdomains connected by flexible loops and short turns (Fig. 2a). Its four subdomains (A-D) are aligned accordingly from the N to C terminus along the MUN<sup>933</sup> structure (Fig. 2a). Subdomains (A-D) consists of helices H1-H2 (A), H3-H6 (B), H7-H11 (C) and H12-H15 (D), respectively (Fig. 2a, b). H7 forms a long and continuous helix that bends and changes direction gradually, with its N-terminal portion packed against the preceding helix H6. MUN<sup>933</sup> is considerably charged, with positive and negative charges widely distributed throughout the surface (Supplementary Fig. 1a). An exposed hydrophobic patch at the junction of subdomains B and C that involves helices H6, H7 and H8 (Supplementary Fig. 1b) is found on the surface of MUN<sup>933</sup>, as discussed in the following sections.

As expected, MUN<sup>933</sup> has a similar architecture to those of vesicle tethering factors such as Sec6p, Tip20, and Exo70, etc<sup>28,31-33</sup> (Fig. 2c). However, MUN<sup>933</sup> adopts a distinctive arch-shaped architecture that differs from the more straight structure of Exo70 and the sharply hooked shape of Tip20. It is unclear whether the overall arch-shape of MUN<sup>933</sup> may result from crystal packing, but this feature might be important for the functional specificity of the MUN domain in synaptic vesicle priming.

### A conserved hydrophobic pocket is key for opening syntaxin-1

Previous studies have shown that Munc13-1 MUN\* stimulates the transition from the Munc18-1-syntaxin-1 complex to the SNARE complex<sup>15</sup>. We thus performed FRET experiments to investigate the activity of MUN<sup>933</sup> in the stimulation (Fig. 3a-e). SNARE assembly reactions started with syntaxin-1 alone or the Munc18-1-syntaxin-1 complex illustrate that Munc18-1 strongly inhibits SNARE complex formation, whereas addition of either MUN\* or MUN<sup>933</sup> equally facilitates SNARE complex assembly (Fig. 3b). This result confirms that MUN<sup>933</sup> is functional in stimulating SNARE complex assembly starting from the Munc18-1-syntaxin-1 complex.

To identify the region of MUN<sup>933</sup> responsible for this activity, we used the solved structure of MUN<sup>933</sup> as a guide and designed several fragments that encompass one or more subdomains of MUN<sup>933</sup>, referred to as MUN-ABC, MUN-BCD, MUN-AB, MUN-BC and MUN-CD (Fig. 1). All these fragments are well-folded and show large  $\alpha$ -helical content as judged from their circular dichroism (CD) spectra (Supplementary Fig. 2a). Among these fragments, MUN-AB and MUN-CD did not stimulate the transition from the Munc18-1-syntaxin-1 complex to the SNARE complex, whereas MUN-ABC, MUN-BCD and MUN-BC exhibited a range of activities in stimulating the transition (Fig. 3c). These results identify subdomains B-C as the core region for MUN<sup>933</sup> activity. Fragments MUN-ABC and MUN-BCD showed relatively higher activities than MUN-BC, but lower than MUN<sup>933</sup>,

suggesting that subdomains A and D play additional albeit less critical roles (compared to subdomains B-C) in stimulating Munc18-1-dependent SNARE complex assembly.

Next, we aimed to identify key residues that mediate the activity of MUN<sup>933</sup>. Based on the MUN<sup>933</sup> structure, we designed a series of mutations on the surface of subdomains B-C (Supplementary Fig. 3a). Using a native gel assay we established (**Online Methods** and Supplementary Fig. 3b) and extensive screening, we found that residues Asn-1128 and Phe-1131 (referred to as NF), are crucial for the activity of MUN<sup>933</sup> in promoting the transition from the Munc18-1–syntaxin-1 complex to the SNARE complex (Supplementary Fig. 3c). FRET experiments confirmed this finding by showing that double mutation of NF to Ala (NFAA) totally disrupted the activity of MUN<sup>933</sup> (Fig. 3d, e). No activity was observed even though the concentration of NFAA was elevated to 100 μM (data not shown), showing the critical importance of the NF sequence. Note also that CD spectroscopy and gel filtration showed that NFAA is well-folded, exhibiting similar CD spectra, denaturation curve and elution volume as MUN<sup>933</sup> (Supplementary Fig. 2b, c). These results rule out the possibility that loss of activity is caused by protein misfolding.

In the structure of MUN<sup>933</sup>, the NF residues reside next to each other on the surface of helix H6 in subdomain B. H6 packs against helices H7 and H8 in an antiparallel and parallel manner, where Met-1127 on H6, Val-1162 and Trp-1165 on H7, and Ile-1215, Ile-1216 and Leu-1219 on H8 form a shallow hydrophobic pocket (Fig. 3f). Thus, this hydrophobic pocket built by these highly conserved residues is formed by residues from subdomains B-C at the junction between the two domains (Fig. 3f), indicating that the loss of function of MUN-AB and MUN-CD arises because the integrity of the hydrophobic pocket is broken. Importantly, sequence alignments showed that residues NF are highly conserved in UNC-13-Munc13s proteins (Fig. 3g). Together, these data show that the hydrophobic pocket, especially the conserved residues NF, are central for the activity of the MUN domain in opening syntaxin-1.

### The NF sequence is crucial for proteoliposome fusion

The FRET experiments showed the importance of the NF sequence for the ability of the MUN domain to mediate the transition from the Munc18-1–syntaxin-1 complex to the SNARE complex in solution. We next sought to verify the key role of the NF sequence in SNARE-mediated membrane fusion.

Our new established *in-vitro* reconstitution assay<sup>25</sup> has recently reproduced the vital functions of Munc18-1 and Munc13-1 in neurotransmitter release. In this assay, instead of using syntaxin-1–SNAP-25 liposomes, we used liposomes reconstituted with Munc18-1–syntaxin-1 complex to start fusion reactions with synaptobrevin-containing liposomes and monitored lipid mixing and content mixing by fluorescence de-quenching methods<sup>25,34</sup>. For these experiments, we used a Munc13-1 fragment that contains the DAG-binding C<sub>1</sub> domain, the PIP2-binding C<sub>2</sub>B domain and the MUN domain [residues 529–1407, EF, 1453–1531; referred to as C<sub>1</sub>-C<sub>2</sub>B-MUN (Fig. 1)] because this fragment is much more efficient than the isolated MUN domain due to the membrane interactions of the C<sub>1</sub> and C<sub>2</sub>B domains<sup>25</sup>. Practically no lipid mixing or content mixing between Munc18-1–syntaxin-1 liposomes and synaptobrevin liposomes were observed when adding SNAP-25 and

syntaptotagmin-1 C<sub>2</sub>AB in the presence of Ca<sup>2+</sup> (Fig. 4a–f). Further addition of 1 μM Munc13-1 C<sub>1</sub>-C<sub>2</sub>B-MUN dramatically facilitated the SNARE-mediated lipid mixing and content mixing (Fig. 4a–f). However, C<sub>1</sub>-C<sub>2</sub>B-MUN containing the NFAA double mutation totally abolished such activity in stimulating both lipid mixing and content mixing (Fig. 4b, e). These data demonstrate that the NF sequence is critical for the activity of Munc13-1 in SNARE-mediated membrane fusion. We also note that C<sub>2</sub>AB was critical to observe content mixing in the experiments with WT C<sub>1</sub>-C<sub>2</sub>B-MUN (Fig. 4e, f), as described previously<sup>25</sup>.

Previous studies have shown that the syntaxin-1 LE mutation that helps opening syntaxin-1 partially rescues release in *unc-13* nulls in *C. elegans* and suppresses the block caused by Munc18-1 in SNARE complex formation, suggesting that UNC-13-Munc13s are involved in opening syntaxin-1<sup>15,23</sup>. In our study, we tested whether the syntaxin-1 LE mutation could rescue membrane fusion in the absence of Munc13-1. Indeed, efficient lipid mixing and content mixing between Munc18-1–syntaxin-1 LE liposomes and synaptobrevin liposomes could still be observed in the absence of Munc13-1 and the presence of SNAP-25, C<sub>2</sub>AB and Ca<sup>2+</sup> (Fig. 4b, e). These data suggest that syntaxin-1 LE mutation reverses the blocking effect caused by Munc18-1 and further support the notion that UNC-13-Munc13s are involved in opening syntaxin-1.

### The NF sequence is pivotal for synaptic vesicle priming

The *in-vitro* experiments above provide strong evidence that the NF sequence of Munc13-1 plays a key role in opening syntaxin-1. Sequence alignments showed that the residues NF are highly conserved in UNC-13-Munc13s from different species (Fig. 3g). To investigate the function of the NF sequence *in vivo*, we took *C. elegans* UNC-13 as a model protein and studied its role in synaptic transmission at cholinergic neuromuscular junctions (NMJs). The *C. elegans* *unc-13* gene is essential for synaptic vesicle exocytosis<sup>35</sup> and encodes long and short isoforms (UNC-13L and S). Both of these two isoforms share a common region that contains the C<sub>1</sub>, C<sub>2</sub>B, MUN and C<sub>2</sub>C domains (Fig. 1). UNC-13L or Munc13s [Munc13-1, -2 (brain-specific)] have an additional N-terminal C<sub>2</sub>A domain and a CaM-binding domain that UNC-13S lacks<sup>36</sup> (Fig. 1). Expression of either UNC-13L or UNC-13S in *unc-13* mutant animals rescued locomotion and neurotransmission defects, indicating that both isoforms are able to restore synaptic vesicle exocytosis<sup>37</sup>. It has also been shown that Munc13s mutants that lack N-terminal C<sub>2</sub>A and CaM-binding domains can rescue the priming defects of synaptic vesicles in the absence of Munc13s<sup>20,38</sup>. Hence, to minimize the complexity, we used the short isoform of UNC-13 (UNC-13S) to assess the role of the NF sequence in synaptic function.

The *s69* allele of *unc-13* corresponds to a 5 base pair deletion in an exon shared by UNC-13S and UNC-13L<sup>39</sup>, which shifts the reading frame thereby inactivating both isoforms. Consistent with previous findings<sup>37</sup>, expression of UNC-13S in *unc-13* (*s69*) rescued the locomotion rate (32.25% of wide-type animals, Supplementary Fig. 4a, b). In contrast, when we mutated the NF residues to Ala (hereafter referred to as UNC-13S NFAA), the mutant failed to rescue the locomotion defects (Supplementary Fig. 4a, b).

To directly characterize the role of the NF sequence in synaptic transmission, we recorded excitatory postsynaptic currents (EPSCs) at NMJs from adult body wall muscles (Fig. 5).

We analyzed both endogenous EPSCs that represent spontaneous fusion of single synaptic vesicle under resting conditions, and evoked EPSCs that represent  $\text{Ca}^{2+}$ -triggered exocytosis of hundreds of synaptic vesicles simultaneously. To minimize variation in recording evoked EPSCs, we employed the optogenetic method by expressing ChR2 in presynaptic neurons and shining blue light (450–490 nm) to depolarize the neurons. *Unc-13 (s69)* null animals exhibited neither spontaneous nor evoked EPSCs. Expressing UNC-13S in *unc-13 (s69)* background rescued endogenous EPSC rate (16.22% of wide type, Fig. 5a, b) and evoked EPSCs (64.73% of wide type, Fig. 5c, d), which is consistent with previous results<sup>37, 40</sup>. In contrast, UNC-13S NFAA mutant completely failed to rescue both endogenous and  $\text{Ca}^{2+}$ -triggered evoked EPSCs (Fig. 5a–d), confirming the vital function of the NF sequence in synaptic vesicle exocytosis.

The defect in presynaptic release of UNC-13S NFAA mutant could be due to defective priming of synaptic vesicles or a defect in response of synaptic vesicles to  $\text{Ca}^{2+}$  influx. A classic assay to analyze priming involves the application of hypertonic sucrose solution to induce synaptic vesicle exocytosis in a  $\text{Ca}^{2+}$ -independent manner, which is often used as a measure of the readily releasable pool (RRP) of vesicles<sup>41</sup>. Here we employed a prolonged sucrose stimulation protocol<sup>41</sup> to release the majority of primed synaptic vesicles at *C. elegans* NMJs. Under this protocol, the sucrose-induced charge transfer observed in wide type and *unc-13 (s69)* were  $21.29 \pm 1.57$  pC and  $4.09 \pm 0.82$  pC during 0–1 s, and  $73.99 \pm 7.78$  pC and  $22.31 \pm 1.83$  pC during 0–5 s (Fig. 5e, f), respectively, comparable to previous results<sup>40, 42</sup>. UNC-13S expression in *unc-13 (s69)* rescued the sucrose-induced charge transfer to  $13.54 \pm 2.68$  pC (63.60% of wide type, Fig. 5e, f) during 0–1 s and  $45.37 \pm 5.15$  pC during 0–5 s stimulation (61.32% of wide type, Fig. 5e, f), whereas the UNC-13S NFAA mutant failed to rescue the sucrose-induced charge transfers ( $3.59 \pm 1.03$  pC, 0–1 s and  $14.58 \pm 5.37$  pC, 0–5 s, Fig. 5e, f). These results reveal that the NF sequence is critical for both spontaneous and evoked release, and indicate a pivotal role for the NF sequence in the priming of synaptic vesicles.

## DISCUSSION

UNC-13-Munc13s perform a crucial function in synaptic vesicle priming, a step prior to  $\text{Ca}^{2+}$ -triggered release that is believed to involve opening of syntaxin-1 and SNARE complex assembly<sup>15, 23</sup>. Previous studies suggested a pathway in which SNARE complex assembly starts with the Munc18-1–syntaxin-1 complex and depends critically on regulation by the Munc13-1 MUN domain<sup>15, 25</sup>. However, the physiological relevance of this model remained unclear, as there was no evidence correlating the priming function of UNC-13-Munc13s *in vivo* with the activity of the MUN domain in opening syntaxin-1 *in vitro*. To bridge the gap between our understanding of the functional properties of the MUN domain and of its molecular features, we solved the crystal structure of the Munc13-1 MUN domain and identified key residues responsible for the activity of the MUN domain in opening syntaxin-1. Moreover, the physiological data demonstrated the critical role of these residues in synaptic vesicle priming. These results provide very strong evidence that the critical function of the MUN domain in the transition of the Munc18-1–syntaxin-1 complex to the SNARE complex underlies the central role of UNC-13-Munc13s in synaptic vesicle priming.

The UNC-13-Munc13 MUN domain has been a long-sought goal because this is the only essential element of the neurotransmitter release machinery for which a three-dimensional structure had not been determined. The crystal structure of *rat* Munc13-1 MUN domain described here reveals an elongated architecture formed by  $\alpha$ -helical bundles, as expected from its predicted homology with tethering factors<sup>26</sup>. The structure enabled us to design a series of mutations in conserved surface residues to probe their importance in the ability of the MUN domain in opening syntaxin-1. By using an *in-vitro* SNARE complex assembly assay, we identified a functionally critical, small hydrophobic pocket located at the junction of subdomains B-C. We showed that two highly conserved residues in this hydrophobic pocket, NF, play a key role in mediating the transition from the Munc18-1–syntaxin-1 complex to the SNARE complex. The NF side chains face the surface of the hydrophobic pocket (Fig. 3f), providing a plausible binding contact for its potential “substrate” (e.g. syntaxin-1 or other SNAREs). Mutation of these residues to alanines (NFAA mutation) does not alter the folding of the MUN domain (Supplementary Fig. 2). Thus, the functional effects of the NFAA mutation must arise from disruption of specific interactions involving these side chains. We characterized these effects at three different levels: (i) SNARE complex assembly in solution; (ii) SNARE-dependent liposome fusion in a reconstituted proteoliposome system; and (iii) synaptic transmission at NMJs in *C. elegans*. The drastic effects of the NFAA mutation at these three levels (Figs. 3d, 4 and 5) demonstrate the vital nature of the NF sequence for MUN domain function and leave little doubt that the impairment caused by this mutation on stimulation of SNARE complex assembly and proteoliposome fusion underlies the abrogation of synaptic vesicle priming caused by the mutation.

The observation that subdomains A and/or D enhance the activity of subdomains B-C in the SNARE complex assembly assay (Fig. 3c, e), suggests that multiple sites of the MUN domain cooperate in catalyzing of syntaxin-1 opening. The multiple interactions underlying the activity of the MUN domain likely involve Munc18-1 in addition to syntaxin-1, as the MUN domain accelerates SNARE complex assembly starting from the Munc18-1–syntaxin-1 complex but not from isolated syntaxin-1<sup>15</sup>. Moreover, in co-flootation assays we observed that the MUN domain binds to liposomes containing reconstituted Munc18-1–syntaxin-1 complex but not liposomes containing isolated syntaxin-1 or syntaxin-1–SNAP-25 complex, and the MUN NFAA mutation disrupted binding to the Munc18-1–syntaxin-1 liposomes (Supplementary Fig. 5). These results suggest that interaction between the MUN domain NF pocket and the Munc18-1–syntaxin-1 complex is key for opening syntaxin-1 and that membrane anchoring enhances the affinity of the MUN domain for the Munc18-1–syntaxin-1 complex. Such enhancement likely arises from weak interactions of basic regions of the MUN domain (see Supplementary Fig. 1a) with the phospholipids. These multiple interactions are likely to underlie the finding that the MUN domain catalyzes not only the transition from the Munc18-1–syntaxin-1 complex to the SNARE complex but also the transition from the syntaxin-1–SNAP-25 complex to the Munc18-1–syntaxin-1 complex, as reported in our previous work<sup>25</sup>. These observations lead us to propose a working model of how UNC-13-Munc13s function (Fig. 6). Briefly, the SNARE complex formation is irreversible once synaptobrevin is available, whereas in the absence of synaptobrevin, there is an equilibrium that is shifted in favor of the Munc18-1–syntaxin-1

complex because it is more stable than the syntaxin-1–SNAP-25 complex. The MUN domain lowers the energy barrier of the transitions between these complexes (see intermediate states).

It is likely that, in addition to mediating opening of syntaxin-1 and SNARE complex assembly, the UNC-13-Munc13 MUN domain has a function in tethering vesicles to presynaptic active zones, since increasing evidence suggests that UNC-13-Munc13s play a role in such tethering<sup>43–45</sup>. This function should be favored by the elongated  $\alpha$ -helix-bundle structure of the Munc13-1 MUN domain, which spans more than 150 Å and is similar to those of factors with known roles in tethering, such as Sec6p, Tip20 and Exo70. We suggest that the function of UNC-13-Munc13s in tethering depends on this elongated  $\alpha$ -helical-bundle structure, and probably on their association with other factors (e.g. RIMs) to form a tethering complex<sup>1</sup>. Nevertheless, structure-based sequence alignments showed that key residues responsible for forming the NF pocket of UNC-13-Munc13s are not shared by other tethering proteins (Supplementary Fig. 6). Hence, these residues likely endow the UNC-13-Munc13 MUN domain with specificity in synaptic vesicle priming.

Further research will be required not only to identify the target of the MUN NF-pocket but also to elucidate the function and molecular mechanism of the MUN domain in tethering. The structure of the Munc13-1 MUN domain structure described here provides a framework to design and interpret these studies.

## ONLINE METHODS

### Recombinant proteins purification

Full-length rat synaptobrevin-2 and its cytoplasmic domain (residues 29–93), full-length rat syntaxin-1a and its cytoplasmic domain (residues 2–253), full-length human SNAP-25A (with its four cysteins mutated to serines) and its SNARE motifs (SN1, residues 11–82; and SN3, residues 141–203), full-length rat Munc18-1, squid Munc18-1, rat Munc13-1 MUN\* domain (residues 859–1407, EF, 1453–1531), C1-C2B-MUN domain (residues 529–1407, EF, 1453–1531), co-expressed Munc18-1–syntaxin-1, and rat synaptotagmin-1 cytoplasmic domain C<sub>2</sub>AB (residues 140–421) were expressed and purified as described previously<sup>8,9,13,15,20,25</sup>. Recombinant rat Munc13-1 MUN<sup>933</sup> (residues 933–1407, EF, 1453–1531) was expressed in BL21 *E. coli* cells as GST fusion protein using a pGEX-KG vector (GE Healthcare). GST-MUN<sup>933</sup> was first purified on a glutathione sepharose 4B (GE Healthcare) affinity column followed by removal of the GST tag with thrombin overnight at 4°C. Further purification was carried out by using successive chromatography steps on Resource Q anion exchange column and Superdex-200 16/600 column (GE Healthcare). Finally, MUN<sup>933</sup> in a buffer containing 20 mM Tris (hydroxymethyl) aminomethane (Tris) pH 8.5, 150 mM NaCl, 10% glycerol (v/v) (buffer A) and 5 mM DL-dithiothreitol (DTT) was concentrated to 9–10 mg/ml for crystallization. Mutants and fragments of MUN domain, including MUN<sup>933</sup> NFAA, MUN-ABC (residues 859–1407), MUN-AB (residues 933–1167), MUN-BCD (residues 1011–1407, EF, 1453–1531), MUN-BC (residues 1011–1407), MUN-CD (residues 1148–1407, EF, 1453–1531) were expressed, purified and concentrated as described for MUN<sup>933</sup>. C1-C2B-MUN NFAA was expressed and purified as

described previously<sup>25</sup> in insect cells (sf9). Protein concentrations were determined by UV-visible spectrometer (SHIMADZU UV-2450). All the reagents were analytical pure grade.

### Protein crystallization and structure determination

Crystals were grown by the hanging drop vapor diffusion method at 4°C. Purified tag-free MUN<sup>933</sup> at 9–10 mg/ml in buffer A and 5 mM DTT was mixed with equal volume of precipitant solution containing 18–25% PEG 3350 (v/v), 0.1 M MES pH 5.8–6.3 and 0.2 M Mg(NO<sub>3</sub>)<sub>2</sub>. Full size crystals were cryoprotected by soaking in harvesting liquor supplemented with 30% glycerol (v/v) before flash cooling in liquid nitrogen. X-ray diffraction data were collected using beamline 19ID [Advanced Photon Source (APS), Argonne National Laboratory, Argonne, IL]. Data were processed with the program HKL2000<sup>46</sup>. The primary model of the MUN<sup>933</sup> was determined by the molecular replacement method using the MUN-CD (PDB entry 3SWH<sup>29</sup>) as starting model. Molecular replacement was performed with the program Phaser<sup>47</sup>. Then a model completion was performed with the pipeline IPCAS (OASIS4.2, available at <http://cryst.iphy.ac.cn>), which gave a result of almost completely model of the protein. The model was manually improved in COOT<sup>48</sup> and iteratively refined by Refmac<sup>49</sup>. In the final model, more than 97% of residues fell in the favored region in the Ramachandran plot and the final *R*<sub>work</sub>/*R*<sub>free</sub> are 0.212/0.252. Data collection and refinement statistics are listed in Table 1.

### Circular dichroism spectroscopy

MUN<sup>933</sup>, its fragments and the mutant NFAA were diluted to a concentration of 0.1 mg/ml in the buffer A and 0.1 mM Tris (2-carboxyethyl) phosphine (TCEP, Sigma-Aldrich). CD spectra were recorded with a JASCO J-810 Spectropolarimeter at 25°C from 200 nm to 250 nm using a 1-mm path-length cuvette. Thermal denaturation was recorded with a MOS-500 Spectropolarimeter (Bio-Logic) at absorption of 222 nm from 25°C to 95°C at 1mm bandwidth.

### Time-based Fluorescence Resonance Energy Transfer (FRET) assay

Rat syntaxin-1 (residues 2–253, C145S, S249C) and human SNAP-25A SN3 (residues 141–203, S187C) were labeled with Tetramethylrhodamine-5-maleimide, single isomer (TMR, Molecular Probe) and BODIPY-FL maleimide (Molecular Probe), respectively. Protein labeling was performed by adding 20-fold molar excess dyes in a buffer containing 20 mM sodium phosphate pH 7.4, 100 mM NaCl (buffer B) and 1 mM TCEP overnight at 4°C. Labeled protein were purified by PD-10 desalting column (GE Healthcare) in a buffer containing 25 mM 4-(2-hydroxyethyl)-1-piperazineethanesulfonic acid (HEPES) pH7.4, 150 mM KCl, 10% glycerol (v/v) (buffer C) and 2 mM DTT (for BODIPY-FL labeled SNAP-25A SN3) or anion exchange chromatography (for TMR labeled syntaxin-1) followed by gel filtration in buffer C to remove free dyes. In the reaction, BODIPY-FL labeled SNAP-25A SN3 was added at a final concentration of 2 μM, TMR labeled syntaxin-1 (pre-incubated or not with squid Munc18) was at 10 μM, MUN\*, MUN<sup>933</sup> and its fragments and mutants were at 30 μM. Each experiment was repeated at least 3 times, FRET efficiency was calculated according to  $E = (F_0 - F_{obs})/F_0$ , where  $F_0$  is the initial fluorescence intensity and  $F_{obs}$  is the fluorescence intensity measured as a function of time. For the

limited solubility of rat Munc18-1, isolated Munc18-1 had to be added at concentrations above 20  $\mu$ M were done with squid Munc18-1, which is more soluble and has a 66.4% sequence identity with rat Munc18-1 as well as very similar biochemical properties<sup>15</sup>.

### Native gel assay

The reactions were initiated by addition of 5  $\mu$ M purified Munc18-1 and syntaxin-1 (residues 2–253) with a protein/protein ratio of 1.2:1, and then incubated with 10  $\mu$ M synaptobrevin-2 (residues 29–93), 10  $\mu$ M SNAP-25A and 30  $\mu$ M MUN<sup>933</sup> or its mutants at room temperature for 2 hours. Non-denaturing gels were prepared using 15% (w/v) polyacrylamide (acrylamide: bisacrylamide, 29:1) for separating gel and 4% (w/v) for stacking gel. The electrophoresis buffer was composed of 25 mM Tris, 250 mM Glycine (pH 8.3). Approximately 5  $\mu$ l of each reaction sample was loaded per well and subjected to electrophoresis overnight at 4°C at 80 V. The complex of Munc18-1 with syntaxin-1 (Munc18–Syx) display sharp and clear bands in native gels, whereas other proteins or complexes show smear bands. Each reaction was repeated at least 3 times and the quantification of the Munc18–Syx complex bands was obtained by Image J (NIH).

### Lipid-mixing and content-mixing assays

Proteoliposomes were prepared using established procedures<sup>25</sup>. Donor (synaptobrevin-2, v-) liposomes contained 60% POPC, 17% POPE, 20% DOPS. Acceptor (Munc18-1–syntaxin-1, t-) liposomes contained 58% POPC, 15% POPE, 20% DOPS, 2% PIP2 and 5% DAG (all phospholipids were purchased from Avanti Polar Lipids). Lipid mixtures were dried in glass tubes with nitrogen gas and followed by vacuum for at least 5 hours. Lipid films were re-suspended in buffer C and 1mM DTT, 1% 3-[*3*-Cholamidopropyl] dimethylammonio] propanesulfonate (CHAPS) (w/v, Amersco) and vortexed for 15 min. Purified proteins in buffer C containing 1% CHAPS (w/v) were added slowly to the micelle at a final concentration of 5 mM total lipids. The protein/lipid ratio for v-liposomes was about 1:500, while the protein/lipid ratio for t-liposomes was about 1:1000. The liposome protein mixtures were incubated at room temperature for 30 min followed by dialyzing against buffer C and 1mM DTT, 1 g/L Bio-beads SM2 (Bio-Rad) 3 times at 4°C in order to remove the detergent extensively. For lipid-mixing assays, v-liposomes (0.25 mM total lipids) containing 1.5% NBD-PE and 1.5% Rhodamine-PE were mixed with t-liposomes (0.5 mM lipids) in the presence of 0.5 ~ 1.0  $\mu$ M C1-C2B-MUN (M13) or C1-C2B-MUN NFAA (M13 NFAA), 5  $\mu$ M SNAP-25A, 2  $\mu$ M C<sub>2</sub>AB fragment (residues 140–421) and/or 0.5 mM Ca<sup>2+</sup> (as indicated in the figures) in a total volume of 60  $\mu$ l. NBD fluorescence emission at 538 nm (excitation 460 nm) was monitored with a PTI QM-40 spectrofluorometer. For content-mixing assays, v-liposomes were dissolved in buffer C containing 1% w/v  $\beta$ -OG and 40 mM sulforhodamine B (Sigma), purified full-length synaptobrevin-2 in buffer containing 1% w/v  $\beta$ -OG was added to the lipid mixtures to make the final concentration of lipids 2mM and the P/L ratio 1:500. The proteoliposome was first dialyzed in small volume in buffer C containing 40 mM sulforhodamine B and followed by dialysis in buffer C containing 1 mM DTT and 1g/L Bio-beads for 3 times at 4°C (2 times 2 hr and one time overnight) for removing free dyes and remnant detergents, t-liposomes were prepared with the same method described for the lipid mixing assays. Content mixing was monitored as described for the lipid mixing assays by measuring de-quenching of sulforhodamine B (excited at 565

nm, emission at 587 nm). The data were analyzed and quantified as described above for the lipid-mixing assays. All experiments were performed at 30 °C for at least 3 times. At the end of each reaction, 1% CHAPS (w/v) was added to solubilize the liposomes. For getting more consistent results, the time traces were converted to  $F_{\text{obs}}/F_0$ , where  $F_{\text{obs}}$  is the observed fluorescence intensity and  $F_0$  is the initial intensity. Then the  $F_{\text{obs}}/F_0$  value observed upon detergent addition for an entire set of experiments has been averaged. This average was finally used to normalize all the traces to display the data as a percentage of maximum fluorescence. The relative efficiencies resulting from different additions were reproducible in separate sets of experiments.

### Liposome co-flootation assay

Munc18-1-syntaxin-1, syntaxin-1 and syntaxin-1–SNAP-25 liposomes containing PC:PE:PS (60%:20%:20%) with a protein/lipid (P/L) ratio of 1:800 were prepared with the same method described for the liposome fusion assays. The liposomes (3.5 mM total lipids) were incubated with 10  $\mu\text{M}$  MUN<sup>933</sup> or MUN<sup>933</sup> NFAA for 3 hours at 16°C. The proteoliposomes and bound proteins were isolated by flotation on a Histodenz density gradient (40%:35%:30%) as previously described<sup>25</sup>. Samples on the top (40  $\mu\text{l}$ ) were taken and analyzed by SDS-PAGE and Coomassie Blue staining.

### Strains

Strain maintenance and genetic manipulation were performed as described<sup>50</sup>. Animals were cultivated at 20°C on agar nematode growth media seeded with OP50 bacteria. The following strains were utilized in this study:

Wild type, N2 bristol  
*unc-13* (s69)  
Ex [Psnb-1::UNC-13S]; *unc-13* (s69)  
Ex [Psnb-1::UNC-13S NFAA]; *unc-13* (s69)  
ST422, zxIs6 [Punc-17::chop-2(H134R)::YFP; LIN-15]  
zxIs6 [Punc-17::chop-2(H134R)::YFP; LIN-15]; *unc-13* (s69)  
Ex [Psnb-1::UNC-13S]; zxIs6 [Punc-17::chop-2(H134R)::YFP; LIN-15]; *unc-13* (s69)  
Ex [Psnb-1::UNC-13S NFAA]; zxIs6 [Punc-17::chop-2(H134R)::YFP; LIN-15]; *unc-13* (s69)

Transgenic strains were isolated by microinjection of various plasmids using *Plin-44*::GFP as coinjection markers. Plasmid coding UNC-13S was a gift from Dr. Kaplan's lab as previously described<sup>37</sup>. For UNC-13S NFAA, amino acid coordinates corresponding to residues N-1128 and F-1131 of Munc13-1 were mutated to alanines in UNC-13S cDNA. For electrophysiological recordings and locomotion behavior assays, transgenes were expressed by the *snb-1* promoter.

### Locomotion and behavior assays

Worm tracking and analysis were performed as previously described<sup>51</sup>. Briefly, worms were reared at 20°C and moved to room temperature 30 min before imaging. Young adult animals were randomly picked to agar plates with no bacterial lawn (30 worms per plate). For Locomotion assay, worms were randomly picked and the locomotion was analyzed 10 min after the worms were removed from food. WAT-902H2 camera (Automatic System, Inc.) was used to capture high-contrast dark-field images of the assay plates. The behavior movies were taped at 1× magnification of a ZEISS V8 microscopy at 25 Hz. These data were analyzed automatically by a home-written object-tracking plugin in Image J (NIH). Locomotion speed and the 30 s crawling trail were achieved by Image J plugin.

### Electrophysiology

Electrophysiology assays were performed at the neuromuscular junctions of dissected *C. elegans* under an Olympus microscope (BX51WI) with an EPC-10 amplifier and Patchmaster software (HEKA) as previously described<sup>52,53</sup>. Recording pipettes were pulled from borosilicate glass capillaries (Sutter Instruments) to a resistance of 3–4 MΩ on a P-97 micropipette puller (Sutter Instruments). Day 2 worms were glued on the surface of Sylgard-coated coverslips using cyanoacrylate-based glue. A dorsolateral incision was made using sharp glass pipettes and cuticle flap was then folded and glued down to the coverslip to expose the body wall muscles. The preparation was treated by collagenase type IV (Sigma-Aldrich) for 30 s at a concentration of 0.4 mg/ml at 20°C. The bath solution contained 127 mM NaCl, 5 mM KCl, 26 mM NaHCO<sub>3</sub>, 1.25 mM NaH<sub>2</sub>PO<sub>4</sub>, 2 mM CaCl<sub>2</sub>, 4 mM MgCl<sub>2</sub>, 10 mM glucose (325–335 mOsm, pH 7.3). The pipette solution contained (in mM) 120 mM CH<sub>3</sub>O<sub>3</sub>SCs, 4 mM CsCl, 15 mM CsF, 4 mM MgCl<sub>2</sub>, 5 mM EGTA, 0.25 mM CaCl<sub>2</sub>, 10 mM HEPES and 4 mM Na<sub>2</sub>ATP (315–325 mOsm, pH 7.2). Membrane potential was clamped at -60 mV. The *zxIs6* strain, in which light-gated cation channel channelrhodopsin-2 (ChR2)-YFP was expressed in cholinergic neurons, was used for recording evoked EPSCs<sup>54</sup>. All-trans retinal was added to the NGM plates at a final concentration of 2.5 μM to mediate light stimulation of ChR2. L4 animals were transferred to NGM plates containing all-trans retinal and the next generation of hermaphrodite adults were used. For RRP depletion, the 0.5 M sucrose in bath solution was applied to ventral nerve cord near the recorded muscles by an IM-300 microinjector (Narishige) with 8 psi for 5 s<sup>40</sup>. Signals were filtered at 2 kHz, sampled at 20 kHz, and analyzed using IGOR Pro software (Wavemetrics).

### Statistical analysis

Statistical significance was determined using a two-tailed Student's *t*-test. Experimental data meet the assumptions of normal distribution. For behavior and electrophysiology assays of worms, the sample size was chosen based on previous studies<sup>37,40</sup> with no inclusion/exclusion criteria. The variances were similar between the groups that are being statistically compared. The investigators were not blinded to the group allocation during the experiments and data analysis.

### Supplementary Material

Refer to Web version on PubMed Central for supplementary material.

## Acknowledgments

We thank the BL19ID station at the APS in Argonne National Laboratory for helping collecting data. We thank J. Kaplan (Massachusetts General Hospital) for providing the *unc-13(s69)* strain; thank the Caenorhabditis Genetic Center for providing other strains used in this work. We thank Y. Li and X. Wang of the Huazhong University of Science and Technology (HUST) for initial efforts to construct MUN domain mutations, M. Zhang (Hong Kong University of Science and Technology) for insightful comments on the manuscript. This work was supported by grant 31370819 from the National Science Foundation of China and grant 2014CB910203 from the National Key Basic Research Program of China (both to C.M.), by grants (31130065, 91313301) from the National Science Foundation of China (both to T.X.), and by grant NS37200 from the US National Institutes of Health (to J.R.).

## REFERENCE LIST

1. Rizo J, Sudhof TC. The Membrane Fusion Enigma: SNAREs, Sec1/Munc18 Proteins, and Their Accomplices-Guilty as Charged? *Annu Rev Cell Dev Biol.* 2012; 28:279–308. [PubMed: 23057743]
2. Toonen RF, Verhage M. Munc18-1 in secretion: lonely Munc joins SNARE team and takes control. *Trends Neurosci.* 2007; 30:564–572. [PubMed: 17956762]
3. Jahn R, Scheller RH. SNAREs—engines for membrane fusion. *Nat Rev Mol Cell Biol.* 2006; 7:631–643. [PubMed: 16912714]
4. Brunger AT, Weninger K, Bowen M, Chu S. Single-molecule studies of the neuronal SNARE fusion machinery. *Annu Rev Biochem.* 2009; 78:903–928. [PubMed: 19489736]
5. Sollner T, Bennett MK, Whiteheart SW, Scheller RH, Rothman JE. A protein assembly-disassembly pathway in vitro that may correspond to sequential steps of synaptic vesicle docking, activation, and fusion. *Cell.* 1993; 75:409–418. [PubMed: 8221884]
6. Hanson PI, Roth R, Morisaki H, Jahn R, Heuser JE. Structure and conformational changes in NSF and its membrane receptor complexes visualized by quick-freeze/deep-etch electron microscopy. *Cell.* 1997; 90:523–535. [PubMed: 9267032]
7. Poirier MA, et al. The synaptic SNARE complex is a parallel four-stranded helical bundle. *Nat Struct Mol Biol.* 1998; 5:765–769.
8. Sutton RB, Fasshauer D, Jahn R, Brunger AT. Crystal structure of a SNARE complex involved in synaptic exocytosis at 2.4 Å resolution. *Nature.* 1998; 395:347–353. [PubMed: 9759724]
9. Dulubova I, et al. A conformational switch in syntaxin during exocytosis: role of munc18. *EMBO J.* 1999; 18:4372–4382. [PubMed: 10449403]
10. Misura KM, Scheller RH, Weis WI. Three-dimensional structure of the neuronal-Sec1-syntaxin 1a complex. *Nature.* 2000; 404:355–362. [PubMed: 10746715]
11. Gerber SH, et al. Conformational switch of syntaxin-1 controls synaptic vesicle fusion. *Science.* 2008; 321:1507–1510. [PubMed: 18703708]
12. Rizo J, Chen X, Arac D. Unraveling the mechanisms of synaptotagmin and SNARE function in neurotransmitter release. *Trends Cell Biol.* 2006; 16:339–350. [PubMed: 16698267]
13. Dulubova I, et al. Munc18-1 binds directly to the neuronal SNARE complex. *Proc Natl Acad Sci USA.* 2007; 104:2697–2702. [PubMed: 17301226]
14. Shen J, Tareste DC, Paumet F, Rothman JE, Melia TJ. Selective activation of cognate SNAREpins by Sec1/Munc18 proteins. *Cell.* 2007; 128:183–195. [PubMed: 17218264]
15. Ma C, Li W, Xu Y, Rizo J. Munc13 mediates the transition from the closed syntaxin-Munc18 complex to the SNARE complex. *Nat Struct Mol Biol.* 2011; 18:542–549. [PubMed: 21499244]
16. Augustin I, Rosenmund C, Sudhof TC, Brose N. Munc13-1 is essential for fusion competence of glutamatergic synaptic vesicles. *Nature.* 1999; 400:457–461. [PubMed: 10440375]
17. Varoqueaux F, et al. Total arrest of spontaneous and evoked synaptic transmission but normal synaptogenesis in the absence of Munc13-mediated vesicle priming. *Proc Natl Acad Sci USA.* 2002; 99:9037–9042. [PubMed: 12070347]
18. Richmond JE, Davis WS, Jorgensen EM. UNC-13 is required for synaptic vesicle fusion in *C. elegans*. *Nat Neurosci.* 1999; 2:959–964. [PubMed: 10526333]

19. Aravamudan B, Fergestad T, Davis WS, Rodesch CK, Broadie K. *Drosophila* UNC-13 is essential for synaptic transmission. *Nat Neurosci.* 1999; 2:965–971. [PubMed: 10526334]

20. Basu J, et al. A minimal domain responsible for Munc13 activity. *Nat Struct Mol Biol.* 2005; 12:1017–1018. [PubMed: 16228007]

21. Madison JM, Nurrish S, Kaplan JM. UNC-13 interaction with syntaxin is required for synaptic transmission. *Curr Biol.* 2005; 15:2236–2242. [PubMed: 16271476]

22. Stevens DR, et al. Identification of the minimal protein domain required for priming activity of Munc13-1. *Curr Biol.* 2005; 15:2243–2248. [PubMed: 16271475]

23. Richmond JE, Weimer RM, Jorgensen EM. An open form of syntaxin bypasses the requirement for UNC-13 in vesicle priming. *Nature.* 2001; 412:338–341. [PubMed: 11460165]

24. Koushika SP, et al. A post-docking role for active zone protein Rim. *Nat Neurosci.* 2001; 4:997–1005. [PubMed: 11559854]

25. Ma C, Su L, Seven AB, Xu Y, Rizo J. Reconstitution of the vital functions of Munc18 and Munc13 in neurotransmitter release. *Science.* 2013; 339:421–425. [PubMed: 23258414]

26. Pei J, Ma C, Rizo J, Grishin NV. Remote homology between Munc13 MUN domain and vesicle tethering complexes. *J Mol Biol.* 2009; 391:509–517. [PubMed: 19563813]

27. Yu IM, Hughson FM. Tethering factors as organizers of intracellular vesicular traffic. *Annu Rev Cell Dev Biol.* 2010; 26:137–156. [PubMed: 19575650]

28. Sivaram MV, Furgason ML, Brewer DN, Munson M. The structure of the exocyst subunit Sec6p defines a conserved architecture with diverse roles. *Nat Struct Mol Biol.* 2006; 13:555–556. [PubMed: 16699513]

29. Li W, et al. The Crystal Structure of a Munc13 C-terminal Module Exhibits a Remarkable Similarity to Vesicle Tethering Factors. *Structure.* 2011; 19:1443–1455. [PubMed: 22000513]

30. Rizo J, Rosenmund C. Synaptic vesicle fusion. *Nat Struct Mol Biol.* 2008; 15:665–674. [PubMed: 18618940]

31. Tripathi A, Ren Y, Jeffrey PD, Hughson FM. Structural characterization of Tip20p and Ds11p, subunits of the Ds11p vesicle tethering complex. *Nat Struct Mol Biol.* 2009; 16:114–123. [PubMed: 19151722]

32. Dong G, Hutagalung AH, Fu C, Novick P, Reinisch KM. The structures of exocyst subunit Exo70p and the Exo84p C-terminal domains reveal a common motif. *Nat Struct Mol Biol.* 2005; 12:1094–1100. [PubMed: 16249794]

33. Moore BA, Robinson HH, Xu Z. The crystal structure of mouse Exo70 reveals unique features of the mammalian exocyst. *J Mol Biol.* 2007; 371:410–421. [PubMed: 17583731]

34. Weber T, et al. SNAREpins: minimal machinery for membrane fusion. *Cell.* 1998; 92:759–772. [PubMed: 9529252]

35. Richmond JE, Davis WS, Jorgensen EM. UNC-13 is required for synaptic vesicle fusion in *C. elegans*. *Nat Neurosci.* 1999; 2:959–964. [PubMed: 10526333]

36. Brose N, Rosenmund C, Rettig J. Regulation of transmitter release by Unc-13 and its homologues. *Curr Opin Neurobiol.* 2000; 10:303–311. [PubMed: 10851170]

37. Hu Z, Tong XJ, Kaplan JM. UNC-13L, UNC-13S, and Tomosyn form a protein code for fast and slow neurotransmitter release in *Caenorhabditis elegans*. *Elife.* 2013; 2:e00967. [PubMed: 23951547]

38. Deng L, Kaeser PS, Xu W, Südhof TC. RIM proteins activate vesicle priming by reversing autoinhibitory homodimerization of Munc13. *Neuron.* 2011; 69:317–331. [PubMed: 21262469]

39. Rose AM, Baillie DL. Genetic organization of the region around UNC-15 (I), a gene affecting paramyosin in *Caenorhabditis elegans*. *Genetics.* 1980; 96:639–648. [PubMed: 7262541]

40. Zhou K, Stawicki TM, Goncharov A, Jin Y. Position of UNC-13 in the active zone regulates synaptic vesicle release probability and release kinetics. *Elife.* 2013; 2:e01180. [PubMed: 24220508]

41. Rosenmund C, Stevens CF. Definition of the readily releasable pool of vesicles at hippocampal synapses. *Neuron.* 1996; 16:1197–1207. [PubMed: 8663996]

42. Gracheva EO, et al. Tomosyn inhibits synaptic vesicle priming in *Caenorhabditis elegans*. *PLoS Biol.* 2006; 4:e261. [PubMed: 16895441]

43. Hammarlund M, Palfreyman MT, Watanabe S, Olsen S, Jorgensen EM. Open syntaxin docks synaptic vesicles. *PLoS Biol.* 2007; 5:e198. [PubMed: 17645391]

44. Siksou L, et al. A common molecular basis for membrane docking and functional priming of synaptic vesicles. *Eur J Neurosci.* 2009; 30:49–56. [PubMed: 19558619]

45. Weimer RM, et al. UNC-13 and UNC-10/rim localize synaptic vesicles to specific membrane domains. *J Neurosci.* 2006; 26:8040–8047. [PubMed: 16885217]

46. Otwinowski Z, Minor W. Processing of X-ray diffraction data collected in oscillation mode. *Methods Enzymol.* 1997; 276:307–326.

47. McCoy AJ, et al. Phaser crystallographic software. *J Appl Crystallogr.* 2007; 40:658–674. [PubMed: 19461840]

48. Emsley P, Lohkamp B, Scott WG, Cowtan K. Features and development of Coot. *Acta Crystallogr D Biol Crystallogr.* 2010; 66:486–501. [PubMed: 20383002]

49. Vagin AA, et al. REFMAC5 dictionary: organisation of prior chemical knowledge and guidelines for its use. *Acta Crystallogr D Biol Crystallogr.* 2004; 60:2184–2195. [PubMed: 15572771]

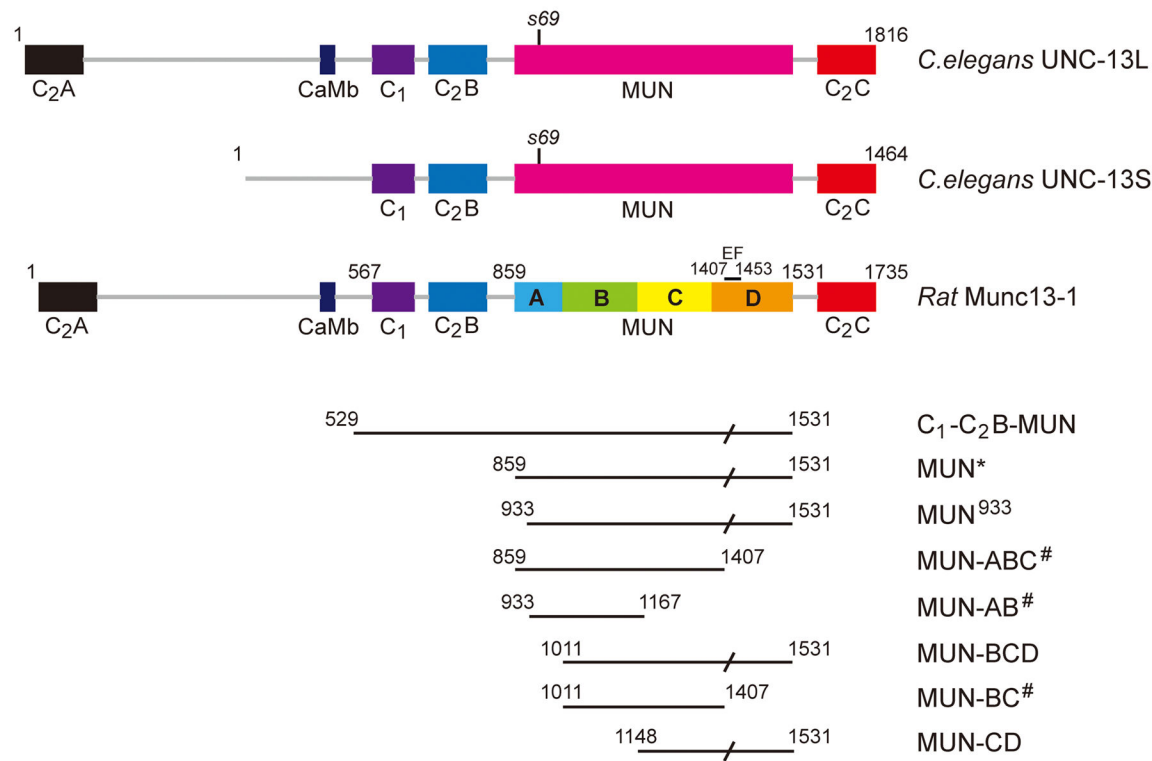
50. Brenner S. The genetics of *Caenorhabditis elegans*. *Genetics.* 1974; 77:71–94. [PubMed: 4366476]

51. Yue Y, et al. The CC1-FHA dimer is essential for KIF1A-mediated axonal transport of synaptic vesicles in *C. elegans*. *Biochem Biophys Res Commun.* 2013; 435:441–446. [PubMed: 23669038]

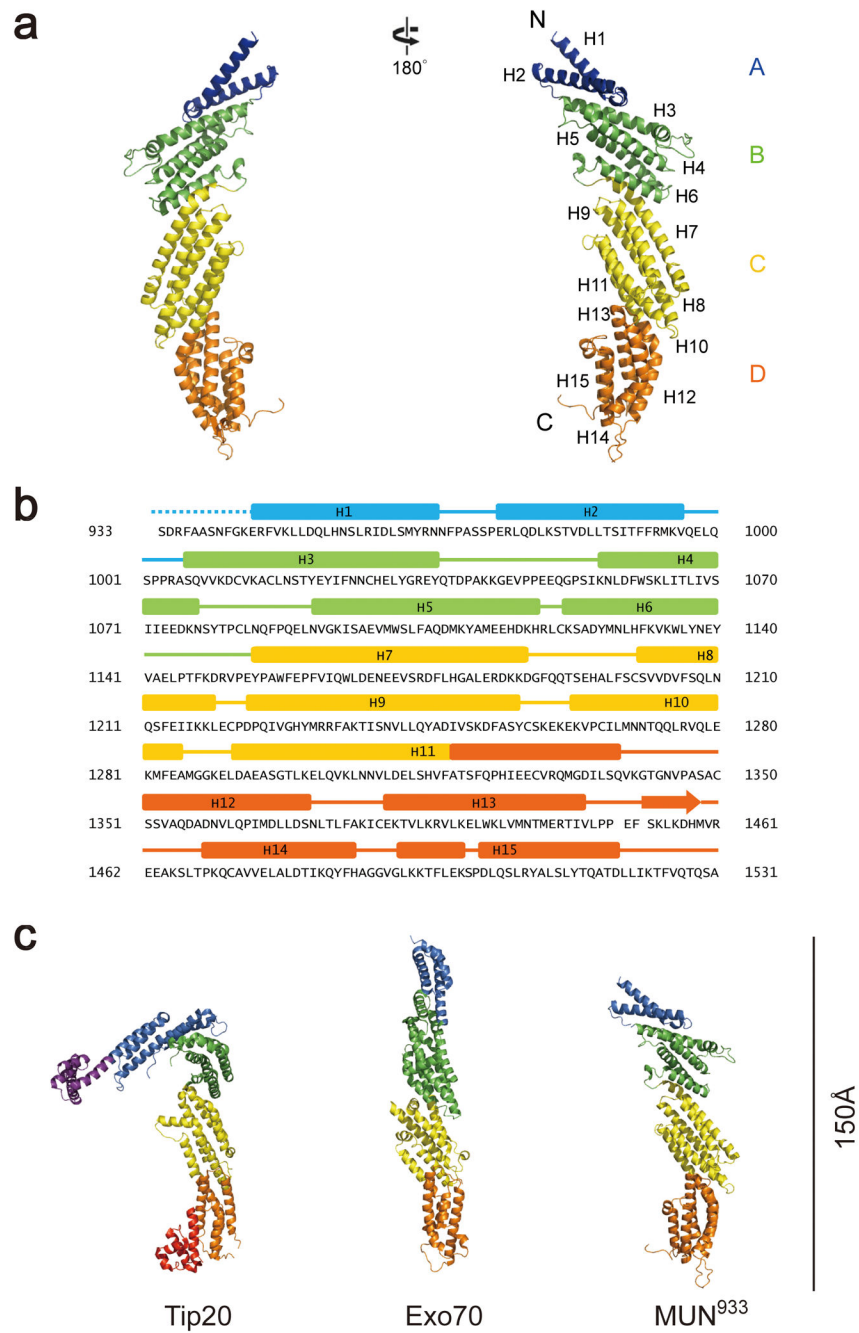
52. Richmond JE, Jorgensen EM. One GABA and two acetylcholine receptors function at the *C. elegans* neuromuscular junction. *Nat Neurosci.* 1999; 2:791–797. [PubMed: 10461217]

53. Kang L, Gao J, Schafer WR, Xie Z, Xu XZ. *C. elegans* TRP family protein TRP-4 is a pore-forming subunit of a native mechanotransduction channel. *Neuron.* 2010; 67:381–391. [PubMed: 20696377]

54. Liewald JF, et al. Optogenetic analysis of synaptic function. *Nat Methods.* 2008; 5:895–902. [PubMed: 18794862]

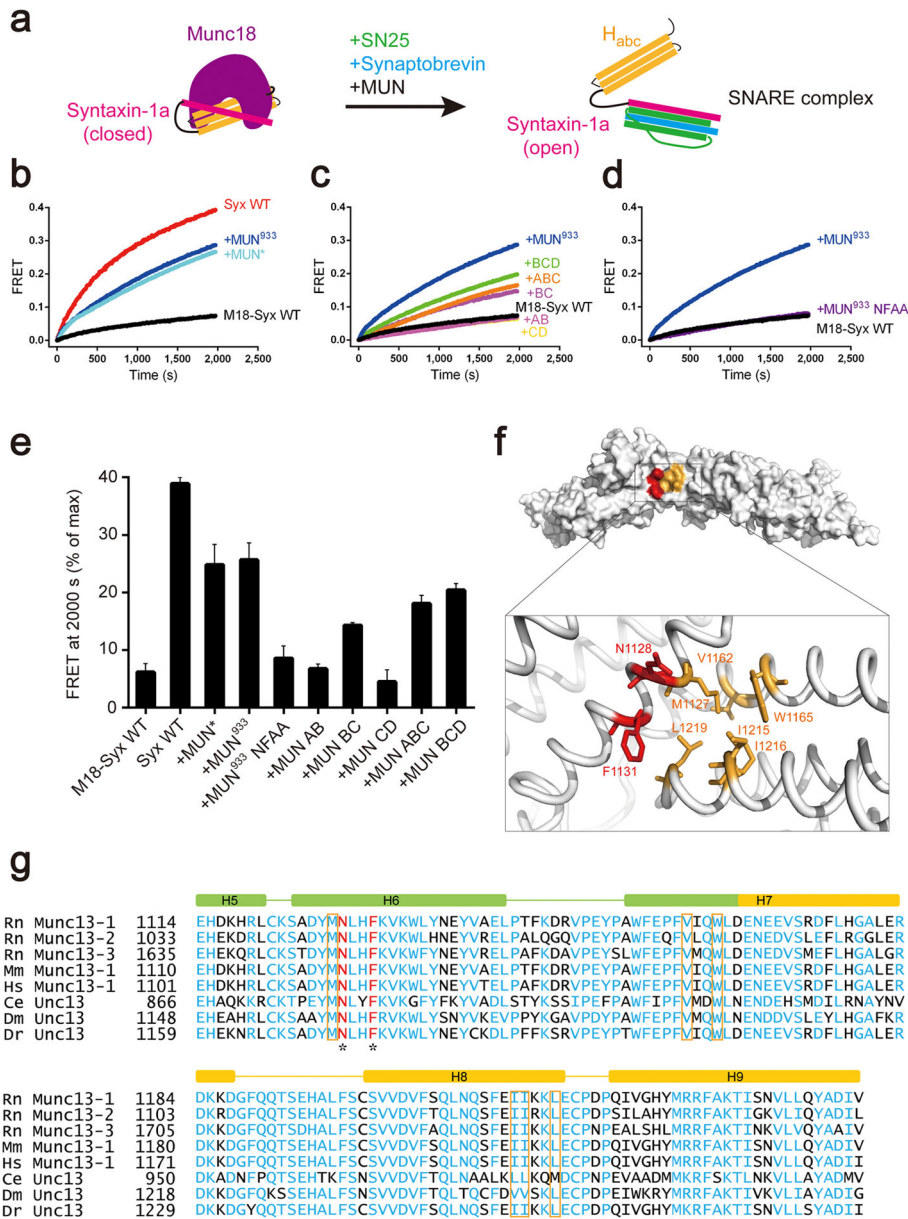
**Figure 1.**

Domain diagrams of UNC-13-Munc13s. The diagrams correspond to *C. elegans* UNC-13L and UNC-13S, and to rat Munc13-1 and its fragments used in this study. The C<sub>2</sub>A, calmodulin-binding (CaMb), C<sub>1</sub>, C<sub>2</sub>B, MUN and C<sub>2</sub>C domains indicated were previously described<sup>20</sup>. The s69 allele corresponds to a 5 base pair deletion in an exon of UNC-13 (exon 21). Residue numbers indicate selected domain and fragments boundaries. The predicted subdomains within the MUN domain are colored in blue, green, yellow and orange and labeled A-D. A long loop of the MUN domain that spans residues 1408–1452 was deleted and replaced with residues Glu (E) and Phe (F), represented by slash. For the proper folding of the fragments indicated by #, the subdomain B and C boundaries are extended to residues 1167 and 1407, respectively, rather than residues 1148 and 1314 defined from the structure. All fragments used are well folded based on analyses by CD spectroscopy (Supplementary Fig. 2a).

**Figure 2.**

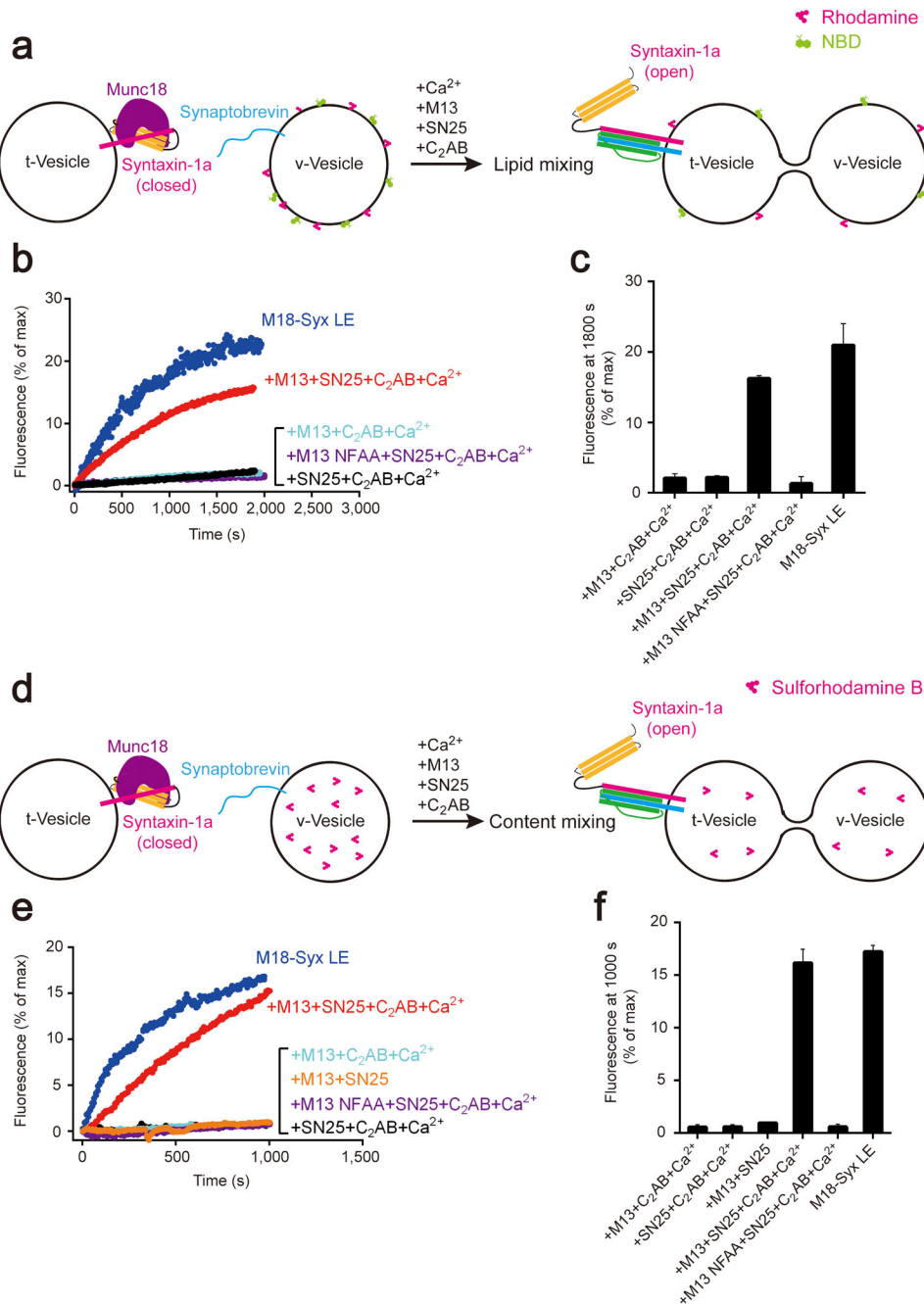
Crystal structure of the Munc13-1 MUN domain. (a) Ribbon diagrams of the crystal structure of MUN<sup>933</sup> shown in two orientations rotated approximately 180° with respect to each other. Subdomains A–D are indicated and colored in blue, green, yellow and orange, respectively. Helices H1–H15 are indicated from the N to the C terminus of the structure. (b) Sequence of MUN<sup>933</sup>. Secondary structure elements are labeled and colored as in a. Dotted lines represent regions in the crystal structure that are either flexible or disordered. (c)

Comparison of the structure of MUN<sup>933</sup> with those of homologous tethering factors that have been solved (i.e. Tip20, PDB entry 3FHN<sup>31</sup>, and Exo70, PDB entry 2PFT<sup>33</sup>).

**Figure 3.**

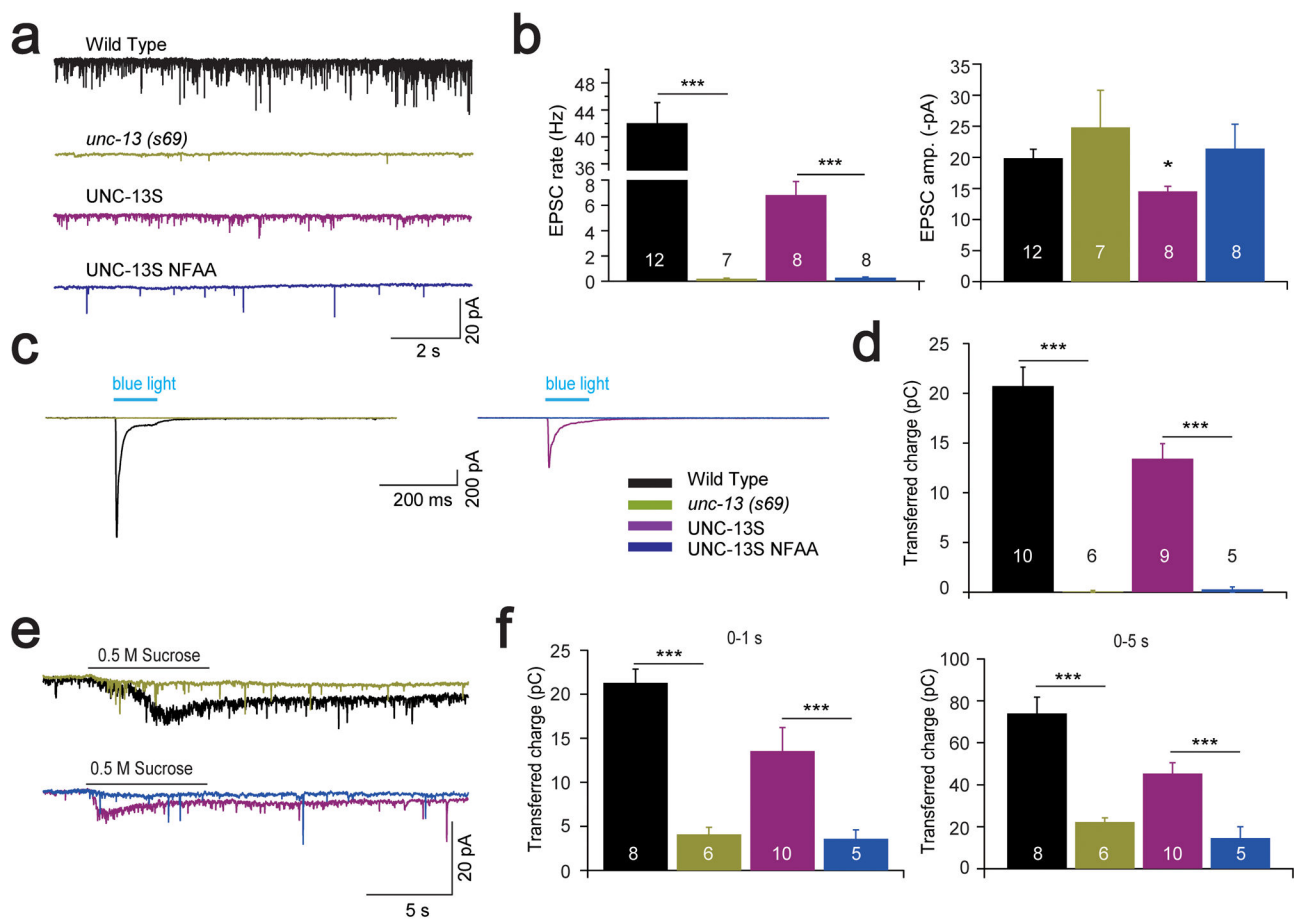
A conserved hydrophobic pocket that mediates the stimulation activity of MUN<sup>933</sup> in the transition from the Munc18-1-syntaxin-1 complex to the SNARE complex. (a) Illustration of SNARE complex assembly FRET assay. (b-d) FRET experiments showing the FRET between a BODIPY FL fluorescence donor on SNAP-25 (SN25) and a rhodamine fluorescence acceptor on syntaxin-1<sub>2-253</sub> within the Munc18-syntaxin-1<sub>2-253</sub> complex (M18-Syx). The stimulation caused by MUN<sup>933</sup>, MUN\*, the MUN<sup>933</sup> fragments and the NFAA mutant are shown. (e) Quantification of the stimulation activities obtained in b-d (data represent mean values,  $\pm$  s.d.; n = 3 technical replicates). (f) Position of the hydrophobic pocket in MUN<sup>933</sup> and enlarged view of its structure. The conserved residues forming the pocket are labeled and colored in yellow, residues N-1128 and F-1131 are

colored in red. (g) Sequence alignment of the hydrophobic pocket region shared in UNC-13-Munc13 species. Residues N-1128 and F-1131 are colored in red and indicated by asterisks, conserved residues in the pocket are labeled in yellow box, other conserved residues are colored in cyan; Rn, *Rattus norvegicus*; Mm, *Mus musculus*; Hs, *Homo sapiens*; Ce, *Caenorhabditis elegans*; Dm, *Drosophila melanogaster*; Dr, *Danio rerio*.

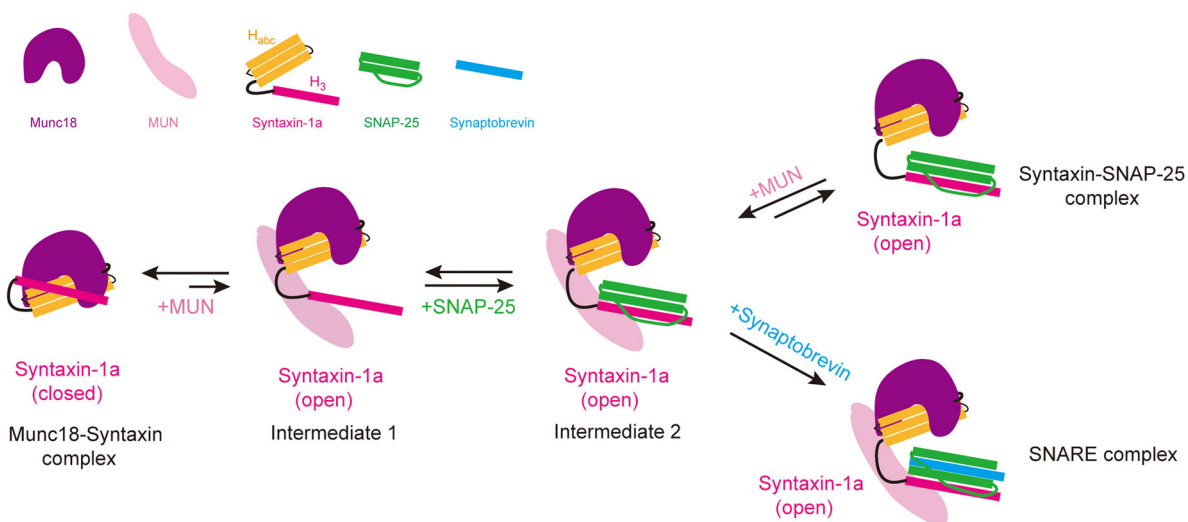
**Figure 4.**

The Munc13-1 NFAA mutation abolishes SNARE-mediated liposome fusion. **(a)** Illustration of the lipid mixing experiment (see **Online Methods**). The donor liposomes (v-liposomes) contain synaptobrevin, while the acceptor liposomes (t-liposomes) contain the Munc18-1-syntaxin-1<sub>1-288</sub> complex or its LE mutant (M18-Syx LE). **(b)** Lipid mixing experiments confirming the critical role of the NF sequence. The experiments were performed in the presence of SNAP-25 (SN25), synaptotagmin-1 cytoplasmic region ( $\text{C}_2\text{AB}$ ),  $\text{C}_1\text{-}\text{C}_2\text{B-MUN}$  (M13) and/or the NFAA mutant, and 0.5 mM  $\text{Ca}^{2+}$  in various

combinations. **(c)** Quantification of the results obtained (data represent mean values,  $\pm$  s.d.;  $n = 3$  technical replicates). **(d)** Illustration of the content mixing experiment (see **Online Methods**) where sulforhodamine fluorescence is de-quenched as donor- and acceptor-liposomes merge. **(e)** Content mixing experiments confirming the critical role of the NF sequence. **(f)** Quantification of the results obtained (data represent mean values,  $\pm$  s.d.;  $n = 3$  technical replicates).

**Figure 5.**

The UNC-13-Munc13 NFAA mutation abolishes synaptic vesicle priming and exocytosis. (a, b) Endogenous EPSCs recording from adult body wall muscles of the indicated genotypes. Representative traces (a) and summary data (b) are shown. (c, d) Photo-evoked EPSCs recording from adult body wall muscles of the indicated genotypes. Averaged traces (c) and the cumulative charge transfer (d) are shown. (e, f) Average recording traces (e) and summary of transferred charges (f) of vesicle release induced by 0.5 M hypertonic sucrose solution in animals of genotype that indicated. Values that differ significantly from controls are indicated (\*\*p < 0.001, \*p < 0.05). For each genotype, independent experiments were carried out in different animals, and the number of animals is indicated in the graph. Error bars indicate s.e.m..

**Figure 6.**

Working model for the mechanism underlying the activity of the MUN domain. The diagrams represent the Munc18-1-syntaxin-1 complex (left), the syntaxin-1-SNAP-25 complex bound to Munc18-1 (upper right) and the SNARE complex bound to Munc18-1 and the MUN domain (lower right), as well as intermediate states that are proposed to mediate the transitions between the different complexes. A key aspect of the model is that multiple weak interactions of the MUN domain with Munc18-1, syntaxin-1 and perhaps the other SNAREs lower the energy barriers involved in these transitions. Starting from the Munc18-1-syntaxin-1 complex, binding of the MUN domain to Munc18-1 and syntaxin-1 is proposed to transiently open syntaxin-1, leading to intermediate 1; binding of SNAP-25 leads to intermediate 2, which can serve as substrate (likely irreversible) for SNARE complex assembly upon synaptobrevin binding. Intermediate 2 could also be in the path leading from the syntaxin-1-SNAP-25 complex to the Munc18-1-syntaxin-1 complex in the absence of synaptobrevin. The relative size of the arrows is meant to illustrate the observation that Munc18-1 displaces SNAP-25 from syntaxin-1. The membranes are not shown but are also expected to influence the equilibria because of interactions with MUN domain and perhaps other components.

**Table 1**

Data collection and refinement statistics (molecular replacement)

<b>Munc13-1 MUN<sup>933</sup></b>	
<b>Data collection</b>	
Space group	P2 <sub>1</sub> 2 <sub>1</sub> 2
Cell dimensions	
<i>a, b, c</i> (Å)	114.1, 270.9, 47.7
$\alpha, \beta, \gamma$ (°)	90.0, 90.0, 90.0
Resolution (Å)	50.0–2.9 (2.95–2.90)
<i>R</i> <sub>merge</sub> (%)	6.9 (63.4)
<i>I</i> / $\sigma$ <i>I</i>	27.3 (1.95)
Completeness (%)	99.3 (98.7)
Redundancy	5.4 (5.1)
<b>Refinement</b>	
Resolution (Å)	50.0–2.9 (2.97–2.90)
No. reflections	32,104 (1,712)
<i>R</i> <sub>work</sub> / <i>R</i> <sub>free</sub>	0.217/0.252
No. atoms	
Protein	4,347
Ligand/ion	–
Water	–
<i>B</i> factors	
Protein	85.4
Ligand/ion	–
Water	–
r.m.s. deviations	
Bond lengths (Å)	0.006
Bond angles (°)	1.384

Values in parentheses are for highest-resolution shell.